

Hedgehog Shaped Microspheres Assembled by Mn₂CuO₄ Nanobelts Decorated on Graphene Oxide for Highly Efficient Sensing of Hydrogen Peroxide

Su-Juan Li*, Zhen-Zhen Qi, Zhi-Wen Luo, Shuang Miao

Henan Province Key Laboratory of New Optoelectronic Functional Materials, College of Chemistry and Chemical Engineering, Anyang Normal University, Anyang, 455000, Henan, China

*E-mail: lemontree88@163.com

Received: 6 December 2021 / Accepted: 27 January 2022 / Published: 4 March 2022

Solvothermal method was used to synthesize a unique nanostructure with hedgehog shaped microspheres assembled by ordered Mn₂CuO₄ nanobelts, which was characterized by SEM, TEM and XRD. These Mn₂CuO₄ microspheres were loaded on graphene oxide (GO) support to form Mn₂CuO₄/GO nanocomposites, and its application for highly efficient sensing of hydrogen peroxide (H₂O₂) was demonstrated. The CV and amperometry results indicated that Mn₂CuO₄/GO nanocomposites exhibited superior electrocatalytic performance over Mn₂CuO₄ for H₂O₂ detection. The developed sensor shows a high detection sensitivity (838.9 $\mu\text{A mM cm}^{-2}$), a wide linear concentration range (0.5-2352 μM), and a low limit of detection (20 nM). In addition, the Mn₂CuO₄/GO based H₂O₂ sensor possesses good reproducibility, stability, selectivity and effective sample application.

Keywords: Manganese copper oxide; Nanobelt; 3D hedgehog shaped microspheres; Hydrogen peroxide; Electrochemical sensor

1. INTRODUCTION

Hydrogen peroxide (H₂O₂), as a typical reactive oxygen species and cellular released byproducts, plays important functions in process of biological metabolism, such as probing the expression of specific oxidase and regulation of cellular signaling pathways [1-2]. Deviation from the normal level of H₂O₂ in body fluids is related with cancer, Alzheimer's disease, Parkinson's disease, and so on [3-5]. Thus, it is imperative to develop new strategies for the accurate and sensitive determination of H₂O₂ concentrations quantitatively. To date, several techniques including spectrophotometry [6], colorimetry [7], chemiluminescence [8] and fluorimetry [9] have been used to determine H₂O₂. With the evolvement of detection strategies, electrochemical methods stand out due to its advantages of rapid response, cost effectiveness, simplicity of operation, high sensitivity and good selectivity for detecting H₂O₂ based on

its oxidation or reduction at electrode surface.

Commonly reported electrochemical H_2O_2 sensors contain enzymatic and nanomaterials based nonenzymatic sensors. The enzymatic sensor shows high detection sensitivity and selectivity for detection of H_2O_2 , but its widespread application is limited by the intrinsic fragility and instability of enzymes [10]. Current efforts have been paid to develop nonenzymatic H_2O_2 sensors employing various nanomaterials on transducer. In this field, searching for suitable nanomaterials with high electrocatalytic activity, low price, rich resource and high conductivity has been the persistent goal. Binary transition metal oxides (BTMOs) have become the intensive focus of the research owing to its outstanding physicochemical properties, for instance, multivalent states and unique crystalline structures. The multivalent cations in BTMOs offer the inherent donor-acceptor active sites to promote the reversible adsorption of H_2O_2 on BTMOs, and thus, the charge-transfer process was facilitated [11]. Compared with the unimetal oxides, an enhanced electric conductance and larger specific surface area were achieved for BTMOs [12,13]. These exciting properties in conjunction with the intimate bonding and possible synergetic coupling effect between the two metals, allowed for BTMOs based electrodes desired electrochemical sensors for H_2O_2 [14,15].

Because of the superior properties, various types of BTMOs were fabricated for application in electrochemical sensors with excellent activity, such as hollow nanostructured CoFe_2O_4 [16], CoMn_2O_4 nanoparticles [17], mesoporous NiCo_2O_4 nanospheres [18], Mn_2CuO_4 microspheres [19] and MnFe_2O_4 nanoparticles [20]. Despite the advances, however, the resultant sensing performance still needs to be further improved. Two common strategies were utilized to meet the challenge of these BTMOs. One is to controllably design novel BTMOs nanostructures with desired shape and size, as the morphology has prominent effect on the performance of electrochemical applications. The other is forming hybrids with suitable supporting materials to optimize the catalytic performance of BTMOs.

Based on the above analysis, in this work, the unique hedgehog shaped microspheres assembled by Mn_2CuO_4 nanobelts were prepared through a facile solvothermal preparation method followed by a subsequent calcination under low temperature. Graphene oxide (GO) was selected as supporting material to decorate Mn_2CuO_4 nanostructures. Here, GO provides several advantages such as, aqueous solution processability, substantial oxygen-containing groups, much edge defects and sites for functionalization. The resultant $\text{Mn}_2\text{CuO}_4/\text{GO}$ nanocomposites were used as electrode material for application in electrochemical sensing of H_2O_2 . The electrocatalytic behavior of H_2O_2 at $\text{Mn}_2\text{CuO}_4/\text{GO}$ nanocomposites was investigated by cyclic voltammetry (CV) and amperometry. The sensing performance of $\text{Mn}_2\text{CuO}_4/\text{GO}$ nanocomposites toward H_2O_2 , including linear concentration range, detection sensitivity and selectivity, response time, reproducibility and stability was also demonstrated.

2. EXPERIMENTAL SECTION

2.1. Reagents and apparatus

H_2O_2 , $\text{Cu}(\text{NO}_3)_2 \cdot 3\text{H}_2\text{O}$, $\text{Mn}(\text{NO}_3)_2 \cdot 4\text{H}_2\text{O}$, K_2HPO_4 , KH_2PO_4 , ethylene glycol (EG) and urea were purchased from Aladdin Chemical Reagent Co., Ltd. (Shanghai, China). Dopamine (DA), glucose,

ascorbic acid (AA) and uric acid (UA) were purchased from Sigma Aldrich. All of these reagents were of analytical grade quality and used directly without further purification. 0.1 M H₂O₂ stock solution was prepared and stored at 4 °C in a refrigerator. Certain volumes of stock solution were diluted with electrolyte to desired concentration of working solutions. Phosphate-buffered solutions (PBS, 0.1 M, pH 7.0) were prepared with 0.1 M K₂HPO₄ and KH₂PO₄. The obtained PBS was utilized as electrolyte solutions throughout the whole experiments. 18.2 MΩ cm deionized water was used for preparing various solutions.

Field emission scanning electron microscope (FESEM, Hitachi SU-8010) and transmission electron microscopy (TEM, Tecnai G2 S-Twin F20) were employed to characterize the morphologies of the Mn₂CuO₄ nanobelts assembled for hedgehog shaped microspheres. The structure and chemical composition of synthesized Mn₂CuO₄ materials were characterized using X-ray diffractometer (XRD Rigaku Ultima III) with a Cu Kα (λ = 1.5418 Å). Electrochemical experiments comprising of cyclic voltammetry (CV) and amperometry were performed on a CHI 660D electrochemical station (Shanghai Chenhua Instrument Co. Ltd., China). The conventional three-electrode system was used with Mn₂CuO₄/GO nanocomposites modified electrode as the working electrode, a platinum wire as auxiliary electrode, and a saturated calomel electrode (SCE) as reference electrode.

2.2. Synthesis of Mn₂CuO₄/GO nanocomposites

First, the unique hedgehog shaped microspheres assembled by Mn₂CuO₄ nanobelts were prepared through a facile solvothermal preparation method followed by a subsequent calcination. The detailed synthetic process is as follows: both 10 mL of 0.05 M Cu(NO₃)₂ and 0.025 M Mn(NO₃)₂ were added to 40 mL of solvent constituted by 3:1 volume ratio of water and EG under constant stirring at 25 °C. Then, stepwise addition of 10 mL 0.1 M urea into the above mixture was performed under continuous stirring until complete dissolution. After that, the resultant reaction solution was quickly transferred to a 100 mL Teflon-lined stainless steel autoclave and heated to 180 °C for retaining 12 h. After cooled to room temperature, the products were obtained by centrifugation and repeatedly washed with deionized water and ethanol, and finally dried at 60 °C for 12 h. The leftovers were calcinated at 400 °C for 2 h in the muffle furnace to obtain Mn₂CuO₄ nanobelts assembled for hedgehog shaped microspheres.

GO was prepared from natural graphite powder through modified Hummers method according to previous report [21]. 2 mg GO and 2 mg Mn₂CuO₄ were added into 2 mL deionized water to form 2 mg/mL Mn₂CuO₄/GO nanocomposites dispersion under the help of ultrasonication.

2.3. Electrochemical detection of H₂O₂ by Mn₂CuO₄/GO nanocomposites modified electrodes

Prior to modification, the bare GCE was polished using 0.3 and 0.05 μm alumina powder sequentially, sonicated with deionized water and ethanol. 6 μL 2 mg mL⁻¹ of Mn₂CuO₄/GO nanocomposites aqueous dispersion was dropped onto the surface of GCE. After dried at room temperature, Mn₂CuO₄/GO nanocomposites modified GCE (Mn₂CuO₄/GO/GCE) was prepared. For comparison study, the Mn₂CuO₄ microsphere modified GCE (Mn₂CuO₄/GCE) and GO modified GCE

(GO/GCE) were also prepared according to the above process similar to that of $\text{Mn}_2\text{CuO}_4/\text{GO}/\text{GCE}$. The following CV experiments were carried out in 0.1 M pH 7.0 PBS spiked with different concentrations of H_2O_2 between -0.5 and 0.2 V at a scan rate of 50 mV s^{-1} . Amperometric curves were recorded in an electrolyte cell with 10 mL PBS contained at an applied potential of -0.4 V.

3. RESULTS AND DISCUSSION

3.1. Structural and morphology characterizations

The morphologies of Mn_2CuO_4 microsphere and $\text{Mn}_2\text{CuO}_4/\text{GO}$ nanocomposites were characterized by FESEM and TEM, which were presented in figure 1 (Fig. 1). As observed from low magnification of SEM images in Fig. 1a, the synthesized Mn_2CuO_4 shows spherelike morphologies and the diameter size of these spheres is in the range of 2~5 μm . The microstructure with rough, porous and unique hedgehog shaped microspheres is assembled by Mn_2CuO_4 nanobelts, which can be seen from the high magnification of SEM images (Fig. 1b and 1c). It is interesting to observe that the width of nanobelts range from several tens of nanometers at the top (sphere surface) to hundreds of nanometers at the bottom (sphere center). The porous structure is arising from the interspace between nanobelts. Such a rough and porous microsphere architecture possesses larger surface area and more reactive sites available than the solid counterparts, which is beneficial for diffusion of analytes to electrode transducer and results in enhanced electrocatalytic performance [22]. From the TEM images of Mn_2CuO_4 (Fig. 1e, 1f), similar nanobelts assembled for microspheres are also presented. Panel g of Fig. 1 show the high-resolution TEM (HRTEM) images, and the interplane spacing of 0.47 and 0.24 nm respectively corresponding to the (111) and (311) planes of Mn_2CuO_4 . After decoration of Mn_2CuO_4 microsphere on GO surface, a thin layer of GO nanosheets was covered onto Mn_2CuO_4 microsphere through possible hydrogen bond and electrostatic interactions to form $\text{Mn}_2\text{CuO}_4/\text{GO}$ nanocomposites (Fig. 1d).

The unique structure of Mn_2CuO_4 nanobelts assembled for microsphere is mainly ascribed to the generation of metal glycolate and gas bubbles. Upon adding the metal salts into EG solvent, metal alkoxides were formed through the coordination bond between the -OH of EG and metal ions of Cu^{2+} and Mn^{2+} [15, 19]. With the temperature increase of the above reaction mixture, the obtained metal glycolates connect each other to form nanobelts structure, then, the nanobelts assembled into microsphere under the interaction of van der Waals force. During solvothermal process, the gas bubbles (NH_3 and CO_2) generated by urea decomposition are formed, which results in the unique porous structure. Generally, the size of gas bubbles increase from the center of material to its surface at the solid-liquid interface, therefore, the width of Mn_2CuO_4 nanobelts ranges from several tens of nanometers at the top to hundreds of nanometers at the bottom. At last, the gas bubbles were released from the Mn_2CuO_4 microspheres in the calcination treatment to achieve Mn_2CuO_4 crystallines.

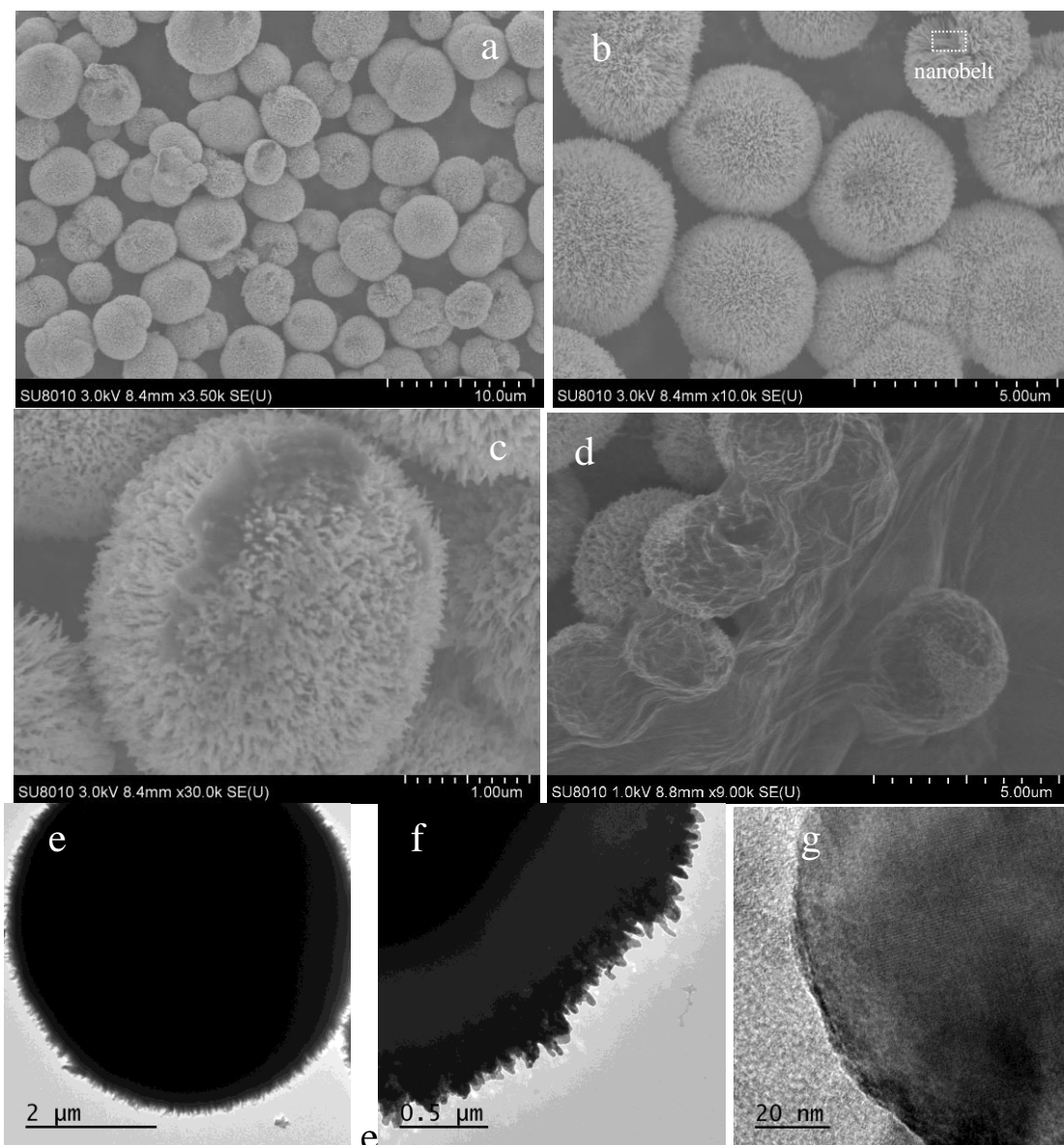


Figure 1. FESEM (a-c), TEM (e-g) images, (g) SAED pattern of Mn_2CuO_4 microspheres, and (d) FESEM images of $\text{Mn}_2\text{CuO}_4/\text{GO}$ nanocomposites.

The XRD patterns of Mn_2CuO_4 microspheres are displayed in Fig. 2 to characterize the crystallinity of MCO. The major diffraction peaks at 2θ of 18.47, 30.39, 35.81, 37.46, 43.52, 47.66, 54, 57.58, 63.25, 71.78, 74.86 and 75.88° correspond to the (111), (220), (311), (222), (400), (331), (422), (511), (440), (620), (533), and (622) respectively. All these diffraction peaks are in good agreement with the crystal planes of cubic Mn_2CuO_4 phase in comparison to standard JCPDS no.076-2296. However, some new peaks can also be observed in XRD patterns of Mn_2CuO_4 microsphere, indicating presence of other possible impurities.

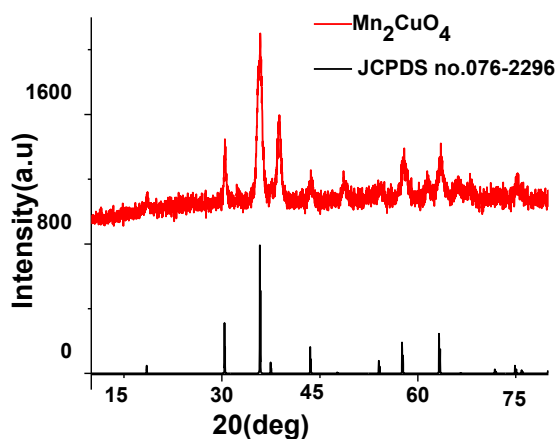


Figure 2. Powder XRD patterns of Mn_2CuO_4 microspheres.

3.2. Electrochemical behaviors of $\text{Mn}_2\text{CuO}_4/\text{GO}$ nanocomposites toward H_2O_2 .

CV was first used to investigate the electrocatalytic properties of the as-prepared $\text{Mn}_2\text{CuO}_4/\text{GO}$ nanocomposites toward the reduction of H_2O_2 . Fig.3 presents the CVs of the bare GCE, GO/GCE , $\text{Mn}_2\text{CuO}_4/\text{GCE}$ and $\text{Mn}_2\text{CuO}_4/\text{GO}/\text{GCE}$ in 0.1 M pH 7.0 PBS without and with 1 mM H_2O_2 involved. It can be seen that for both bare GCE and GO/GCE , when 1 mM H_2O_2 are injected into the PBS solution, the current response shows no obvious change, compared to the corresponding ones without H_2O_2 . These reveals that the GCE substrate and modification of GO have negligible catalytic activity for the electroreduction of H_2O_2 . In addition, there is no obvious redox peak in the present potential scan range for both bare GCE and GO/GCE . However, the $\text{Mn}_2\text{CuO}_4/\text{GCE}$ and $\text{Mn}_2\text{CuO}_4/\text{GO}/\text{GCE}$ exhibit a strong redox couple located at potentials of about -0.19/-0.05 V and -0.18/-0.04 V, respectively, in the PBS solution. Such redox couple is ascribed to electrochemical conversion of $\text{Cu(II)}/\text{Cu(I)}$ in Mn_2CuO_4 microspheres [23]. In the presence of 1 mM H_2O_2 , an obvious increase of the cathodic peak currents can be seen, indicating the high electrochemical catalytic activities of Mn_2CuO_4 and $\text{Mn}_2\text{CuO}_4/\text{GO}$ nanocomposites toward H_2O_2 . Compared the CV curves of $\text{Mn}_2\text{CuO}_4/\text{GCE}$ and $\text{Mn}_2\text{CuO}_4/\text{GO}/\text{GCE}$, the increased cathodic peak currents produced by H_2O_2 for $\text{Mn}_2\text{CuO}_4/\text{GO}$ is much higher than that for only Mn_2CuO_4 , suggesting the significant role of GO for promoting the electrochemical activities of Mn_2CuO_4 . Here, the doping of less electron affinitive Mn is reported to enhance catalytic activities of $\text{Cu(II)}/\text{Cu(I)}$ redox couple toward the reduction of H_2O_2 to H_2O through reducing the energy barrier for O-O cleavage [19].

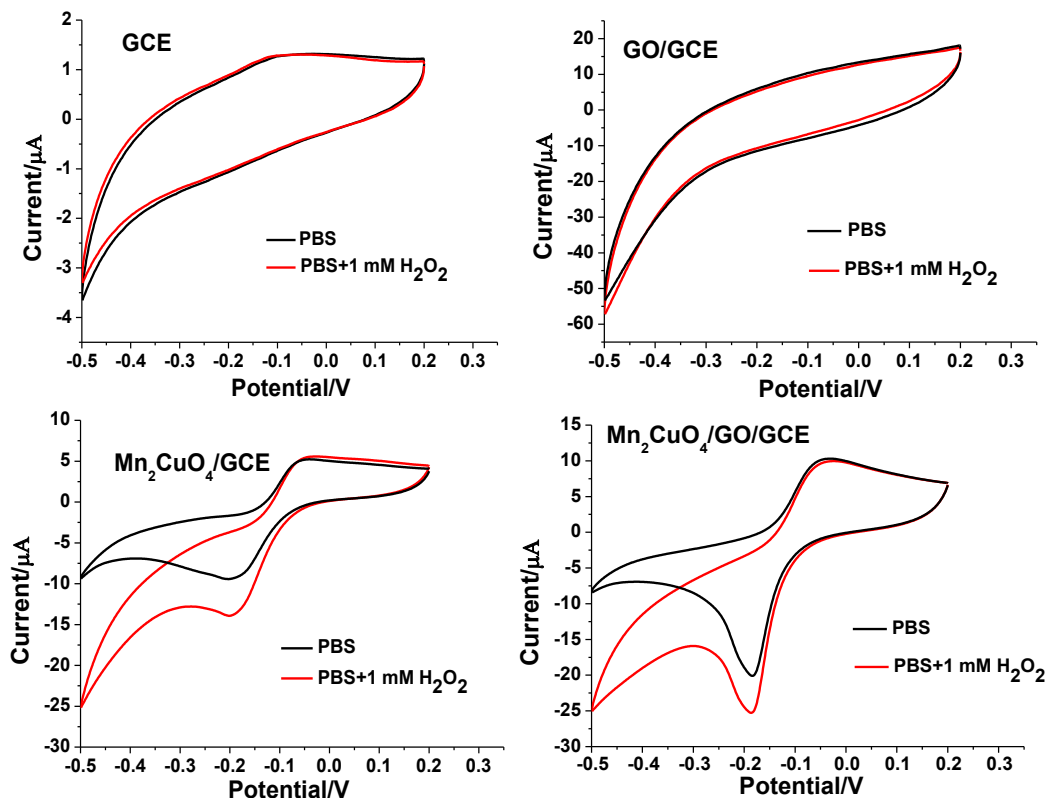


Figure 3. CV curves of bare GCE, GO/GCE, Mn₂CuO₄/GCE and Mn₂CuO₄/GO/GCE in 0.1 M pH 7.0 PBS at a scan rate of 50 mV s⁻¹ without (black curve) and with (red curve) 1 mM H₂O₂ involved.

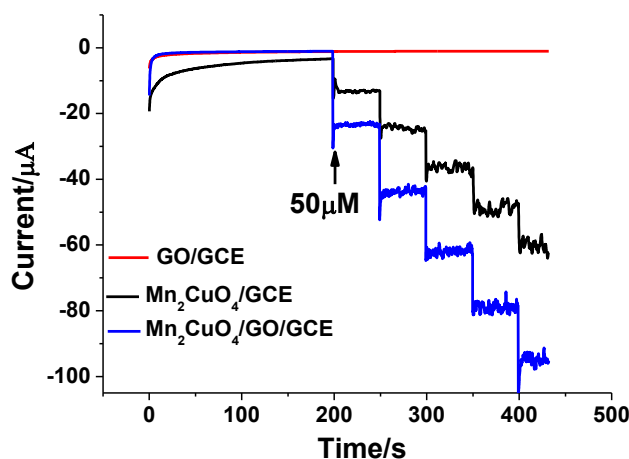


Figure 4. Amperometric responses of GO/GCE, Mn₂CuO₄/GCE and Mn₂CuO₄/GO/GCE with stepwise additions of 50 μM H₂O₂ in 0.1 M pH 7.0 PBS at applied potential of -0.4 V.

To further confirm the priority of Mn₂CuO₄/GO naocomposites toward H₂O₂ detection, amperometric responses of GO/GCE, Mn₂CuO₄/GCE and Mn₂CuO₄/GO/GCE with stepwise additions of 50 μM H₂O₂ in 0.1 M pH 7.0 PBS at applied potential of -0.4 V were compared, the results of which is presented in Fig. 4. As observed, the addition of H₂O₂ results in no obvious current change for GO/GCE, but a distinct increase in the reduction current was observed for Mn₂CuO₄/GCE and Mn₂CuO₄/GO/GCE, and the current response of Mn₂CuO₄/GO/GCE is approximately 1.6 times larger

than that of $\text{Mn}_2\text{CuO}_4/\text{GCE}$, indicating the prominent role of GO for enhancing the detection sensitivity of $\text{Mn}_2\text{CuO}_4/\text{GO}$ nanocomposites toward H_2O_2 .

To investigate the type of controlled process for electrochemical reduction of H_2O_2 , the influence of scan rate on the cathodic peak current was studied by recording CVs of $\text{Mn}_2\text{CuO}_4/\text{GO}/\text{GCE}$ in 0.1 M pH 7.0 PBS with presence of 1 mM H_2O_2 at different scan rates. As can be seen in Fig.5, the cathodic peak currents increased with increasing scan rate from 20 to 200 mV s^{-1} . The plot between cathodic peak current and square root of scan rate shows good linearity with a correlation coefficient of $R=0.9975$ (inset of Fig. 5), indicating a diffusion controlled electrochemical process.

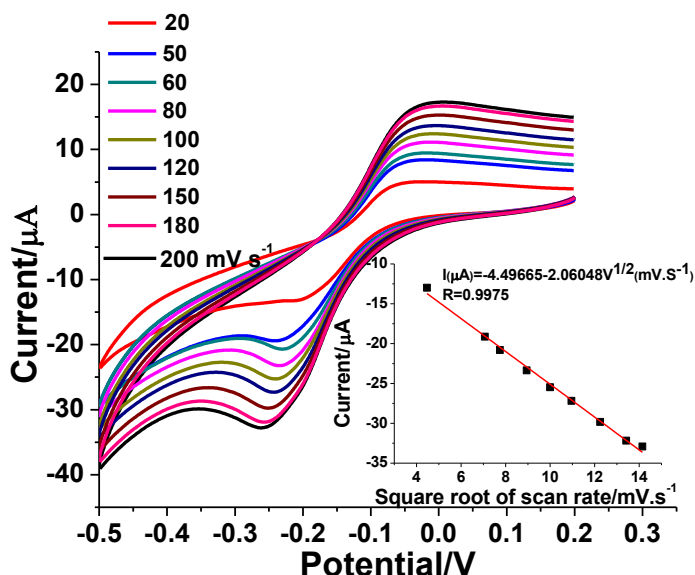


Figure 5. CV curves of $\text{Mn}_2\text{CuO}_4/\text{GO}/\text{GCE}$ in 0.1 M pH 7.0 PBS with presence of 1 mM H_2O_2 at different scan rate ranging from 20 to 200 mV.s^{-1} .

3.3. Amperometric performance of $\text{Mn}_2\text{CuO}_4/\text{GO}$ nanocomposites toward H_2O_2

To obtain the analytical performance of the $\text{Mn}_2\text{CuO}_4/\text{GO}$ nanocomposites based sensor for H_2O_2 detection, the amperometric measurement was carried out. Fig. 6 shows the typical amperometric currents of $\text{Mn}_2\text{CuO}_4/\text{GO}/\text{GCE}$ and $\text{Mn}_2\text{CuO}_4/\text{GCE}$ on successive additions of different concentrations of H_2O_2 into 0.1 M pH 7.0 stirred PBS at an applied potential of -0.4 V. During the analysis performed with $\text{Mn}_2\text{CuO}_4/\text{GO}/\text{GCE}$, the cathodic current increases accordingly with stepped increase of the H_2O_2 concentration (Fig.6a). $\text{Mn}_2\text{CuO}_4/\text{GO}/\text{GCE}$ reached 90% of the steady-state current within 3~5 s, suggesting a fast response to H_2O_2 . From the calibration curve shown in Fig.6b, the response current of $\text{Mn}_2\text{CuO}_4/\text{GO}/\text{GCE}$ is linearly proportional to H_2O_2 concentration in the range of 0.5 μM to 2352 μM with the linear regression equation of $I(\mu\text{A})=2.43624+0.05927C(\mu\text{M})$ (correlation coefficient of 0.9997). While for $\text{Mn}_2\text{CuO}_4/\text{GCE}$ (Fig.6c and 6d), the linear concentration range is 1~10362 μM and the obtained calibration curve can be expressed as $I(\mu\text{A})=0.96578-0.03711C(\mu\text{M})$ with linear correlation coefficient of 0.9994. According to the slope of the calibration curve, the detection sensitivity can be

calculated to be 838.9 and 525.3 $\mu\text{A mM cm}^{-2}$ for $\text{Mn}_2\text{CuO}_4/\text{GO}/\text{GCE}$ and $\text{Mn}_2\text{CuO}_4/\text{GCE}$, respectively. Based on criterion of $S/N=3$, the limit of detection (LOD) for $\text{Mn}_2\text{CuO}_4/\text{GO}/\text{GCE}$ and $\text{Mn}_2\text{CuO}_4/\text{GCE}$ is estimated to be 20 nM and 1 μM , respectively. Compared the analytical performance of the two materials for sensing H_2O_2 , though the linear concentration range of $\text{Mn}_2\text{CuO}_4/\text{GO}/\text{GCE}$ is lower than $\text{Mn}_2\text{CuO}_4/\text{GCE}$, both the high detection sensitivity and low detection limit of $\text{Mn}_2\text{CuO}_4/\text{GO}/\text{GCE}$ is of more priority. The possible reason is as follows: First, the intimate contact between Mn_2CuO_4 and GO through possible hydrogen bond and electrostatic interactions can improve the electron transfer to target H_2O_2 and enhance its electrochemical response; Second, as a highly efficient connector between porous Mn_2CuO_4 microspheres, GO with nanosheet structure provide large surface area and makes more exposed active sites of Mn_2CuO_4 available toward analyte of H_2O_2 ; Third, the abundant oxygen-containing groups of GO facilitate the firmly loading of $\text{Mn}_2\text{CuO}_4/\text{GO}$ on substrate electrode surface, circumventing the falling off of Mn_2CuO_4 microspheres from the electrode surface.

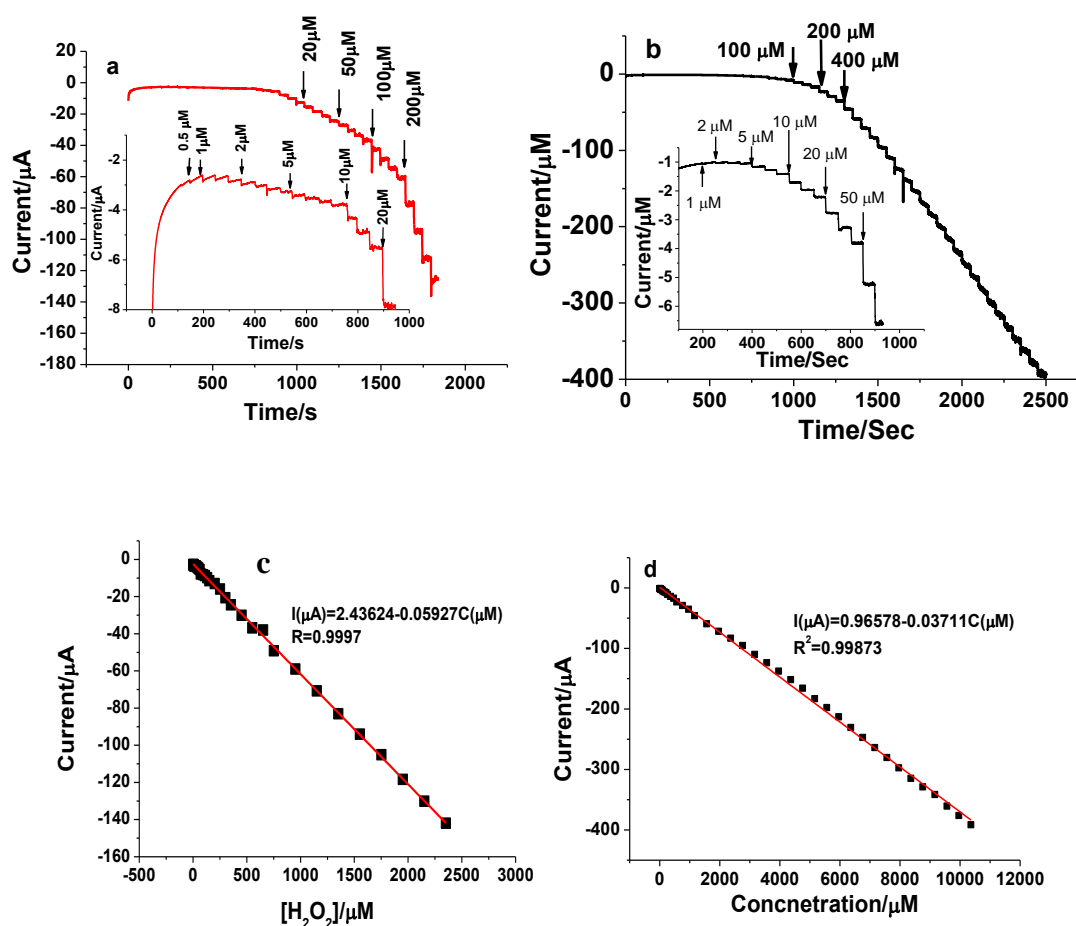


Figure 6. Amperometric responses of $\text{Mn}_2\text{CuO}_4/\text{GO}/\text{GCE}$ (a) and $\text{Mn}_2\text{CuO}_4/\text{GCE}$ (b) on successive additions of different concentrations of H_2O_2 into 0.1 M pH 7.0 PBS at an applied potential of -0.4 V (Inset: current response of H_2O_2 at lower concentrations), and the obtained calibration curves of $\text{Mn}_2\text{CuO}_4/\text{GO}/\text{GCE}$ (c) and $\text{Mn}_2\text{CuO}_4/\text{GCE}$ (d) for H_2O_2 detection.

The comparison of the analytical performance of the present $\text{Mn}_2\text{CuO}_4/\text{GO}$ nanocomposites for

H₂O₂ detection with other previously reported H₂O₂ sensors is shown in Table 1. As observed, the present sensor exhibits superior or comparable characteristics than most of the H₂O₂ sensors given in Table 1.

Table 1. Comparison of the analytical performance of various materials toward electrochemical detection of H₂O₂.

materials	linear range (μM)	detection sensitivity ($\mu\text{A } \mu\text{M}^{-1} \text{cm}^{-2}$)	LOD (μM)	reference
3D GO–Co ₃ O ₄ PHs	0.015	3450	0.05–400 450–1250	24
Fe ₃ O ₄ nanodots	2.5-6540	191.57	1.1	25
AuNWs/PDMS	40-15000	250	12	26
2D Cu ₂ O-rGO-P	5-10560	-	3.78	23
AP-Ni-MOF	4-60000	-	0.9	27
Mn ₂ CuO ₄	0.036–9300	3107	0.013	19
AuPt/ZIF-8-rGO	0.1–18000	-	0.019	28
Mn ₂ CuO ₄ /GO	0.5-2352	838.9	0.02	This work

3.4. Reproducibility, stability and interference of Mn₂CuO₄/GO nanocomposites modified Electrode.

To assess the reproducibility of the Mn₂CuO₄/GO/GCE, five electrodes were fabricated with the same procedure and then their current responses toward 50 μM H₂O₂ were compared by amperometry. The results showed that the current responses of the different five electrodes were reproducible, with a relative standard deviation (RSD) of only 4.3%. The storage stability of the Mn₂CuO₄/GO/GCE was also investigated by periodically monitoring its amperometric current toward 50 μM H₂O₂ by the same Mn₂CuO₄/GO/GCE for 2 week. When not for use, the electrode was stored in 4 °C refrigerator. After 2 weeks, only 4.8% decrease of the current responses for H₂O₂ was obtained, indicating excellent stability of Mn₂CuO₄/GO/GCE.

The interference effect of some common interferent species such as AA, DA, UA, glucose, urea and KCl, NaCl on the specificity of present sensor for H₂O₂ was investigated at -0.4 V in 0.1 M pH 7.0 PBS. The amperometric currents of Mn₂CuO₄/GO/GCE toward the additions of 200 μM of the above interferent species were compared with that obtained for analyte of 50 μM H₂O₂. As observed from Fig.7, a remarkable current is produced by 50 μM H₂O₂, but the current responses of these interferent species can nearly be negligible compared to that of H₂O₂, and the presence of these biological substance has totally no effect on the subsequent response of H₂O₂, indicating a satisfactory selectivity of the Mn₂CuO₄/GO/GCE to H₂O₂.

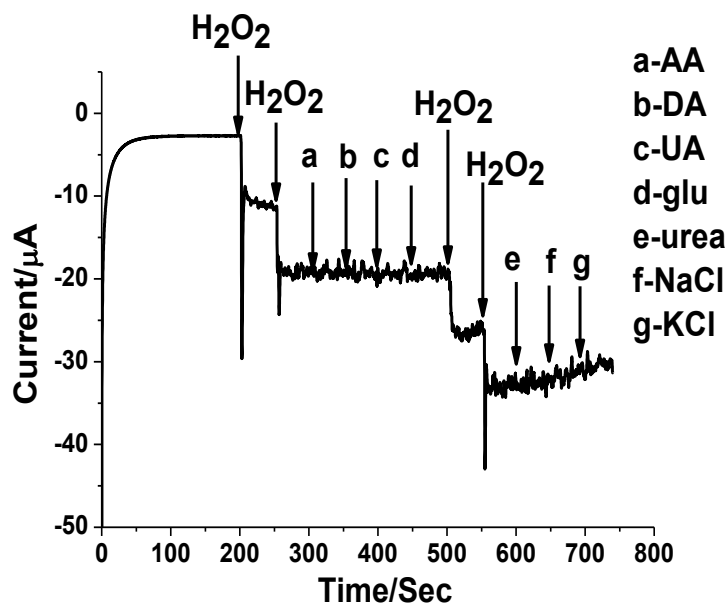


Figure 7. Amperometric responses of $\text{Mn}_2\text{CuO}_4/\text{GO}/\text{GCE}$ with additions of $50 \mu\text{M H}_2\text{O}_2$, $50 \mu\text{M H}_2\text{O}_2$, $200 \mu\text{M AA}$, $200 \mu\text{M DA}$, $200 \mu\text{M UA}$, $200 \mu\text{M glucose}$, $50 \mu\text{M H}_2\text{O}_2$, $50 \mu\text{M H}_2\text{O}_2$, $200 \mu\text{M urea}$, $200 \mu\text{M NaCl}$, and $200 \mu\text{M KCl}$ in $0.1 \text{ M pH } 7.0 \text{ PBS}$ at an applied potential of -0.4 V .

3.5. Real sample analysis.

The practical application of the developed sensor was checked by using sample of disinfectant containing 3% H_2O_2 . The sample was first spiked into $0.1 \text{ M pH } 7.0 \text{ PBS}$ and its current response was measured by amperometry. Different amounts of H_2O_2 standard solution were added into the sample, and quantitative analysis was performed by using standard addition method. Every current value was measured for three times for all samples. The obtained recoveries are listed in Table 2. The recoveries range from 97.6% to 105.8% and the RSD values are acceptable, indicated that the present sensor has potential prospect for determination of H_2O_2 in real samples.

Table 2. Determination of H_2O_2 in real samples.

Samples	Found before added (mM)	added (mM)	Found after added (mM)	RSD(%)	Recovery (%)
1	0.4348	0.1000	0.5239	4.2	98.1
2	0.4336	0.3000	0.7511	3.8	105.8
3	0.4355	0.6000	1.0208	4.6	97.6

4. CONCLUSIONS

In this work, the fabrication of a highly sensitive and selective nonenzymatic sensor based on GO supported Mn_2CuO_4 microspheres for determination of H_2O_2 is described. The Mn_2CuO_4 with unique hedgehog shaped microspheres assembled by ordered nanobelts was prepared by a solvothermal

method, and its integration with GO was achieved under possible hydrogen bond and electrostatic interactions. The electrochemical results exhibited that Mn₂CuO₄/GO nanocomposites have superior electrocatalytic activity over Mn₂CuO₄ toward the reduction of H₂O₂, indicating the significant role of GO for improving the sensing performance of nanocomposites. The obtained Mn₂CuO₄/GO sensor shows a linear range of 0.5 μ M to 2352 μ M, a high detection sensitivity of 838.9 μ A mM cm⁻² and a low LOD with 20 nM. In addition, the developed sensor have a good specificity toward H₂O₂ detection, some common biological and inorganic substances present with H₂O₂ have nearly no interference. The effective application of this sensor in real sample of disinfectant was also demonstrated. The feasibility of this work may enable the application of such a low-cost Mn₂CuO₄/GO platform for detecting various electrochemical species or even biomolecules.

References

1. W. Chen, S. Cai, Q.Q. Ren, W. Wen, Y.D. Zhao, *Analyst*, 137 (2012) 49.
2. C. Li, R. Wu, J. Zou, T. Zhang, S. Zhang, Z. Zhang, X. Hu, Y. Yan, X. Ling, *Biosens. Bioelectron.*, 116 (2018) 81.
3. M. Asif, H. Liu, A. Aziz, H. Wang, Z. Wang, M. Ajmal, F. Xiao, H. Liu, *Biosens. Bioelectron.*, 97 (2017) 352.
4. D. Pramanik, S.G. Dey, *J. Am. Chem. Soc.*, 133 (2011) 81.
5. Y. Wei, Y. Zhang, Z. Liu, M. Guo, *Chem. Commun.*, 46 (2010) 4472.
6. A. Lobnik, M. Cajlakovic, *Sens. Actuators B: Chem.*, 74 (2001) 194.
7. J. Kosman, B. Juskowiak, *Anal. Chim. Acta*, 707 (2011) 7.
8. J. Yuan, A.M. Shiller, *Anal. Chem.*, 71 (1999) 1975.
9. Q. Lu, J. Wang, B. Li, C. Weng, X. Li, W. Yang, X. Yan, J. Hong, W. Zhu, X. Zhou, *Anal. Chem.*, 92 (2020) 7770.
10. F. Meng, X. Yan, J. Liu, J. Gu, Z. Zou, *Electrochim. Acta*, 56 (2011) 4657.
11. C. Yuan, H.B. Wu, Y. Xie, X.W. Lou, *Angew. Chem. Int. Ed.*, 53 (2014) 1488.
12. Y. Wang, Z. Nie, X. Li, Y. Zhao, H. Wang, *Sens. Actuators B: Chem.*, 346 (2021) 130539.
13. Z.L. Wu, C.K. Li, F.W. Zhu, S. Liao, J.G. Yu, H. Yang, X.Q. Chen, *Sens. Actuators B: Chem.*, 253 (2017) 949.
14. W. Cai, J. Lai, T. Lai, H. Xie, J. Ye, *Sens. Actuators B: Chem.*, 224 (2016) 225.
15. P. Balasubramanian, T.S.T. Balamurugan, S.M. Chen, T.W. Chen, *J. Hazard. Mater.*, 361 (2019) 123.
16. K. Vasuki, K.J. Babu, S. Sheet, G. Siva, A.R. Kim, D.J. Yoo, G.G. Kumar, *Microchim. Acta*, 184 (2017) 2579.
17. W. Liu, Z. Zhou, L. Yin, Y. Zhu, J. Zhao, B. Zhu, L. Zheng, Q. Jin, *Sens. Actuators B: Chem.*, 271 (2018) 247.
18. J. Zhang, Q. Mei, Y. Ding, K. Guo, X. Yang, J. Zhao, *ACS Appl. Mater. Interfaces*, 9 (2017) 29771.
19. P. Balasubramanian, M. Annalakshmi, S.M. Chen, T. Sathesh, T.K. Peng, T.S.T. Balamurugan, *ACS Appl. Mater. Interfaces*, 10 (2018) 43543.
20. S. Sahoo, P.K. Sahoo, A. Sharma, A.K. Satpati, *Sens. Actuators B: Chem.*, 309 (2020) 127763.
21. M. Choucair, P. Thordarson, J.A. Stride, *Nature Nano*, 4 (2009) 30.
22. S.J. Li, W. Guo, B.Q. Yuan, D.J. Zhang, Z.Q. Feng, J.M. Du, *Sens. Actuators B: Chem.*, 240 (2017) 398.
23. C. Cheng, C. Zhang, X. Gao, Z. Zhuang, C. Du, W. Chen, *Anal. Chem.*, 90 (2018) 1983.
24. K. Sakthivel, M. Govindasamy, S.M. Chen, A. Muthumariappan, V. Mani, S. Selvaraj, *Sens. Actuators B: Chem.*, 253 (2017) 773.

25. S.Z. Bas, C. Cummins, D. Borah, M. Ozmen, M.A. Morris, *Anal. Chem.*, 90 (2018) 1122.
26. Q. Lyu, Q. Zhai, J. Dyson, S. Gong, Y. Zhao, Y. Ling, R. Chandrasekaran, D. Dong, W. Cheng, *Anal. Chem.*, 91 (2019) 13521.
27. B. Sherino, S. Mohamad, S.N.A. Halim, N.S.A. Manan, *Sens. Actuators B: Chem.*, 254 (2018) 1148.
28. T. Zhang, Y. Xing, Y. Song, Y. Gu, X. Yan, N. Lu, H. Liu, Z. Xu, H. Xu, Z. Zhang, M. Yang, *Anal. Chem.*, 91 (2019) 10589.

© 2022 The Authors. Published by ESG (www.electrochemsci.org). This article is an open access article distributed under the terms and conditions of the Creative Commons Attribution license (<http://creativecommons.org/licenses/by/4.0/>).